

DOI: 10.1002/open.201300009

Nonlinear d^{10} - ML_2 Transition-Metal Complexes

Lando P. Wolters^[a] and F. Matthias Bickelhaupt^{*[a, b]}

We have investigated the molecular geometries of a series of dicoordinated d^{10} -transition-metal complexes ML_2 ($M = Co^-$, Rh^- , Ir^- , Ni , Pd , Pt , Cu^+ , Ag^+ , Au^+ ; $L = NH_3$, PH_3 , CO) using relativistic density functional theory (DFT) at ZORA-BLYP/TZ2P. Not all complexes have the expected linear ligand–metal–ligand ($L-M-L$) angle: this angle varies from 180° to 128.6° as a function of the metal as well as the ligands. Our main objective is to present a detailed explanation why ML_2 complexes can become bent. To this end, we have analyzed the bonding mechanism in ML_2 as a function of the $L-M-L$ angle using

quantitative Kohn–Sham molecular orbital (MO) theory in combination with an energy decomposition analysis (EDA) scheme. The origin of bent $L-M-L$ structures is π backdonation. In situations of strong π backdonation, smaller angles increase the overlap of the ligand's acceptor orbital with a higher-energy donor orbital on the metal–ligand fragment, and therefore favor π backdonation, resulting in additional stabilization. The angle of the complexes thus depends on the balance between this additional stabilization and increased steric repulsion that occurs as the complexes are bent.

Introduction

Dicoordinated d^{10} -transition-metal complexes ML_2 occur in numerous catalytic reaction mechanisms.^[1] These complexes, in general, have a linear geometry^[2,3,4,5] with a ligand–metal–ligand ($L-M-L'$) angle (or bite angle) of 180° , although exceptions^[6,7] have been observed. This geometrical preference can be easily understood for a closed-shell d^{10} configuration. In most cases, the dominant bonding orbital interaction is σ donation from the ligand's lone-pair orbitals into the empty metal $(n+1)s$ atomic orbital (AO), which has a ligand–metal bond overlap that is independent of the $L-M-L'$ angle (see Figure 1).^[8] At the same time, the steric repulsion associated with a $L...L'$ overlap between the lone pairs (and other closed shells) of the two ligands yields a force that maximizes their mutual distance and thus yields the well-known linear $L-M-L'$ arrangement.

The same conclusion is obtained if one uses valence shell electron pair repulsion (VSEPR) theory adapted for treating transition-metal complexes,^[9,10] or more sophisticated methods based on molecular orbital (MO) theory. Proceeding from the latter, one can deduce the preference for linear over bent ML_2



Figure 1. σ Donation has no preference (left, middle) whereas sterics favor linear $L-M-L$ (right).

complexes from the number of electrons in the valence orbitals and the dependence of the orbital energies on the geometrical parameter of interest (here, the $L-M-L$ angle) in Walsh diagrams.^[8] These diagrams show again that dicoordinate d^{10} -transition-metal complexes, for example, $Ag(NH_3)_2^+$, adopt a linear geometry due to the significant destabilization of the metal d_{xz} AO by the ligand's lone-pair orbitals in combination with steric repulsion between the latter upon bending (see below). Nearly all instances with substantial deviations of the $L-M-L$ bite angle from linearity are complexes in which this distortion is imposed by the structural constraints in bidentate ligands in which a bridge or scaffold forces the two coordinating centers L towards each other.^[1b-d]

In this work, we show that d^{10} - ML_2 complexes are not necessarily linear and may even have a pronounced intrinsic preference to adopt a nonlinear equilibrium geometry. To this end, we have investigated the molecular geometries and electronic structure of a series of d^{10} - ML_2 complexes ($M = Co^-$, Rh^- , Ir^- , Ni , Pd , Pt , Cu^+ , Ag^+ , Au^+ ; $L = NH_3$, PH_3 , CO) using relativistic density functional theory (DFT). Simple d^{10} - ML_2 complexes are found with substantial deviations from linearity, featuring bite angles as small as 131° or even less. All that is necessary for bent d^{10} - ML_2 complexes to occur is sufficiently strong π backdonation. This emerges from our detailed metal–ligand bonding analyses in the conceptual framework of quantitative MO theory contained in Kohn–Sham DFT. The analyses explain the phenomenon and provide a tool for rationally tuning the bite

[a] L. P. Wolters, Prof. Dr. F. M. Bickelhaupt
Department of Theoretical Chemistry and
Amsterdam Center for Multiscale Modeling, VU University
De Boelelaan 1083, 1081 HV Amsterdam (The Netherlands)

[b] Prof. Dr. F. M. Bickelhaupt
Institute for Molecules and Materials
Radboud University Nijmegen
Heyendaalseweg 135, 6525 AJ Nijmegen (The Netherlands)
E-mail: F.M.Bickelhaupt@vu.nl

Supporting information for this article is available on the WWW under <http://dx.doi.org/10.1002/open.201300009>.

© 2013 The Authors. Published by Wiley-VCH Verlag GmbH & Co. KGaA. This is an open access article under the terms of the Creative Commons Attribution Non-Commercial License, which permits use, distribution and reproduction in any medium, provided the original work is properly cited and is not used for commercial purposes.

angle. Based on our analyses, we can augment the text-book Walsh diagram for bending ML_2 complexes involving only σ donation with an extended Walsh diagram that also includes π backbonding.

Theoretical Methods

Computational details: All calculations were carried out using the Amsterdam Density Functional (ADF) program developed by Baerends and co-workers^[11,12,13] The numerical integration was performed using the procedure developed by te Velde et al.^[14] The molecular orbitals (MOs) were expanded in a large uncontracted set of Slater-type orbitals (STOs): TZ2P (no Gaussian functions are involved). The TZ2P basis set^[15] is of triple- ζ quality for all atoms and has been augmented with two sets of polarization functions, that is, 2p and 3d on H, 3d and 4f on C, N, O and P, 4p and 4f on Co, Ni, Cu, 5p and 4f on Rh, Pd and Ag and 6p and 5f on Ir, Pt and Au. An auxiliary set of s, p, d, f and g STOs was used to fit the molecular density and to represent the Coulomb and exchange potentials accurately in each self-consistent field (SCF) cycle. All electrons are included in the variational treatment (no frozen-core approximation used).

Equilibrium structures were obtained by optimizations using analytical gradient techniques.^[16] Geometries and energies were calculated at the BLYP level of the generalized gradient approximation (GGA): exchange is described by Slater's $X\alpha$ potential,^[17] with nonlocal corrections due to Becke^[18] added self-consistently, and correlation is treated using the gradient-corrected functional of Lee, Yang and Parr.^[19] Scalar relativistic effects were accounted for using the zeroth-order regular approximation (ZORA).^[20] This approach has been extensively tested and was shown to agree well with high-level coupled-cluster reference data.^[21] Energy minima have been verified through vibrational analysis.^[22] All minima were found to have zero imaginary frequencies. The PyFrag program was used to facilitate the analyses of the bonding mechanism as a function of the L–M–L angle.^[23]

Bond energy analysis: The bond energy ΔE is decomposed into the strain energy ΔE_{strain} that is associated with the geometrical deformation of the fragments as the bond formation takes place, plus the actual interaction energy ΔE_{int} between the deformed fragments [Equation (1)].

$$\Delta E = \Delta E_{\text{strain}} + \Delta E_{\text{int}} \quad (1)$$

The interaction energy $\Delta E_{\text{int}}(\zeta)$ between two molecular fragments is analyzed as a function of the bite angle ζ in the conceptual framework provided by the Kohn–Sham MO method.^[24] To this end, it is decomposed in

three physically meaningful terms [Eq. (2)] using a quantitative energy decomposition scheme developed by Ziegler and Rauk.^[25]

$$\Delta E_{\text{int}}(\zeta) = \Delta V_{\text{elstat}}(\zeta) + \Delta E_{\text{Pauli}}(\zeta) + \Delta E_{\text{oi}}(\zeta) \quad (2)$$

The term ΔV_{elstat} corresponds to the classical electrostatic interaction between the unperturbed charge distributions $\rho_A(r) + \rho_B(r)$ of the prepared or deformed fragments A and B (see below for definition of the fragments) that adopt their positions in the overall molecule AB, and is usually attractive. The Pauli repulsion term ΔE_{Pauli} comprises the destabilizing interactions between occupied orbitals and is responsible for the steric repulsion. This repulsion is caused by the fact that two electrons with the same spin cannot occupy the same region in space. It arises as the energy change associated with the transition from the superposition of the unperturbed electron densities $\rho_A(r) + \rho_B(r)$ of the geometrically deformed but isolated fragments A and B, to the wavefunction $\Psi^0 = N\hat{A}[\Psi_A\Psi_B]$, that properly obeys the Pauli principle through explicit antisymmetrization (\hat{A} operator) and renormalization (N constant) of the product of fragment wavefunctions (see Ref. [24] for an exhaustive discussion). The orbital interaction ΔE_{oi} accounts for charge transfer (interaction between occupied orbitals on one fragment with unoccupied orbitals on the other fragment, including the HOMO–LUMO interactions) and polarization (empty-occupied orbital mixing on one fragment due to the presence of another fragment). It can be further divided into contributions from each irreducible representation Γ of the interacting system [Eq. (3)].

$$\Delta E_{\text{oi}}(\zeta) = \sum_r \Delta E_{\text{oi}}^r(\zeta) \quad (3)$$

Results and Discussion

Structure and energetics

Structural and energetic data emerging from our ZORA-BLYP/TZ2P computations are collected in Tables 1–4. Most ML_2 complexes have a linear L–M–L angle, which leads to either D_{3h} -

| Table 1. L–M–L angle [°] and linearization energy ΔE_{lin} [kcal mol ⁻¹] in dicoordinate d ¹⁰ - ML_2 complexes. ^[a] | | | | | | | | |
|--|---------|--------------------------------------|-----------------------------------|--------------------------------------|-------|--|-------|---|
| | Group 9 | | Group 10 | | | Group 11 | | |
| | L–M–L | $\Delta E_{\text{lin}}^{\text{[b]}}$ | L–M–L | $\Delta E_{\text{lin}}^{\text{[b]}}$ | L–M–L | $\Delta E_{\text{lin}}^{\text{[b]}}$ | | |
| Co(NH ₃) ₂ ⁻ | 180.0 | 0 | Ni(NH ₃) ₂ | 180.0 | 0 | Cu(NH ₃) ₂ ⁺ | 180.0 | 0 |
| Co(PH ₃) ₂ ⁻ | 131.8 | 6.4 | Ni(PH ₃) ₂ | 180.0 | 0 | Cu(PH ₃) ₂ ⁺ | 180.0 | 0 |
| Co(CO) ₂ ⁻ | 128.6 | 19.9 | Ni(CO) ₂ | 144.5 | 2.1 | Cu(CO) ₂ ⁺ | 180.0 | 0 |
| Rh(NH ₃) ₂ ⁻ | 180.0 | 0 | Pd(NH ₃) ₂ | 180.0 | 0 | Ag(NH ₃) ₂ ⁺ | 180.0 | 0 |
| Rh(PH ₃) ₂ ⁻ | 141.2 | 2.0 | Pd(PH ₃) ₂ | 180.0 | 0 | Ag(PH ₃) ₂ ⁺ | 180.0 | 0 |
| Rh(CO) ₂ ⁻ | 130.8 | 10.2 | Pd(CO) ₂ | 155.6 | 0.5 | Ag(CO) ₂ ⁺ | 180.0 | 0 |
| Ir(NH ₃) ₂ ⁻ | 180.0 | 0 | Pt(NH ₃) ₂ | 180.0 | 0 | Au(NH ₃) ₂ ⁺ | 180.0 | 0 |
| Ir(PH ₃) ₂ ⁻ | 144.1 | 2.4 | Pt(PH ₃) ₂ | 180.0 | 0 | Au(PH ₃) ₂ ⁺ | 180.0 | 0 |
| Ir(CO) ₂ ⁻ | 134.2 | 13.4 | Pt(CO) ₂ | 159.0 | 0.6 | Au(CO) ₂ ⁺ | 180.0 | 0 |

[a] Computed at ZORA-BLYP/TZ2P. [b] Relative energy of the linear ML_2 complex relative to its equilibrium geometry.

Table 2. M–L bond length [Å] and BDE [kcal mol⁻¹] in monocoordinate d¹⁰-ML and dicoordinate d¹⁰-ML₂ complexes.^[a]

| | M–L | BDE | | M–L | BDE | | M–L | BDE |
|---|-------|-------|--|-------|-------|--|-------|------|
| CoNH ₃ ^{-(b,c)} | 1.845 | 217.1 | NiNH ₃ ^[c] | 1.827 | 77.0 | CuNH ₃ ⁺ | 1.911 | 70.0 |
| CoPH ₃ ^{-(b,c)} | 1.971 | 240.6 | NiPH ₃ ^[c] | 1.979 | 88.0 | CuPH ₃ ⁺ | 2.163 | 68.7 |
| CoCO ^{-(b,c)} | 1.630 | 280.6 | NiCO ^[c] | 1.663 | 109.3 | CuCO ⁺ | 1.833 | 50.2 |
| Co(NH ₃) ₂ ^{-(b,c)} | 1.908 | 24.0 | Ni(NH ₃) ₂ ^[c] | 1.888 | 36.2 | Cu(NH ₃) ₂ ⁺ | 1.919 | 61.1 |
| Co(PH ₃) ₂ ^{-(c)} | 2.051 | 48.2 | Ni(PH ₃) ₂ ^[c] | 2.108 | 36.3 | Cu(PH ₃) ₂ ⁺ | 2.232 | 48.0 |
| Co(CO) ₂ ^{-(c)} | 1.715 | 76.3 | Ni(CO) ₂ ^[c] | 1.765 | 48.6 | Cu(CO) ₂ ⁺ | 1.882 | 45.0 |
| RhNH ₃ ^{-(c)} | 2.001 | 55.5 | PdNH ₃ | 2.115 | 21.6 | AgNH ₃ ⁺ | 2.212 | 48.7 |
| RhPH ₃ ^{-(c)} | 2.068 | 89.9 | PdPH ₃ | 2.172 | 39.4 | AgPH ₃ ⁺ | 2.415 | 47.9 |
| RhCO ^{-(c)} | 1.750 | 122.0 | PdCO | 1.861 | 47.4 | AgCO ⁺ | 2.137 | 28.4 |
| Rh(NH ₃) ₂ ^{-(c)} | 2.089 | 22.6 | Pd(NH ₃) ₂ | 2.106 | 28.6 | Ag(NH ₃) ₂ ⁺ | 2.172 | 45.2 |
| Rh(PH ₃) ₂ ^{-(c)} | 2.196 | 38.2 | Pd(PH ₃) ₂ | 2.287 | 28.6 | Ag(PH ₃) ₂ ⁺ | 2.444 | 38.1 |
| Rh(CO) ₂ ^{-(c)} | 1.866 | 58.1 | Pd(CO) ₂ | 1.949 | 34.7 | Ag(CO) ₂ ⁺ | 2.113 | 30.7 |
| IrNH ₃ ^{-(c)} | 1.967 | 85.0 | PtNH ₃ ^[c] | 1.981 | 50.1 | AuNH ₃ ⁺ | 2.085 | 71.4 |
| IrPH ₃ ^{-(c)} | 2.056 | 126.5 | PtPH ₃ ^[c] | 2.095 | 77.3 | AuPH ₃ ⁺ | 2.240 | 84.2 |
| IrCO ^{-(c)} | 1.734 | 166.3 | PtCO ^[c] | 1.776 | 87.9 | AuCO ⁺ | 1.927 | 55.0 |
| Ir(NH ₃) ₂ ^{-(b,c)} | 2.071 | 23.6 | Pt(NH ₃) ₂ ^[c] | 2.061 | 41.6 | Au(NH ₃) ₂ ⁺ | 2.088 | 64.6 |
| Ir(PH ₃) ₂ ^{-(c)} | 2.190 | 44.1 | Pt(PH ₃) ₂ ^[c] | 2.249 | 38.7 | Au(PH ₃) ₂ ⁺ | 2.351 | 52.6 |
| Ir(CO) ₂ ^{-(c)} | 1.854 | 66.3 | Pt(CO) ₂ ^[c] | 1.911 | 47.1 | Au(CO) ₂ ⁺ | 2.002 | 40.4 |

[a] Computed at ZORA-BLYP/TZ2P. Bond dissociation energies (BDEs) are given for the complexes in the electronic configuration corresponding to a d¹⁰s⁰ electron configuration and relative to closed-shell d¹⁰s⁰ metal atoms. [b] The d¹⁰s⁰-type configuration is an excited state of the complex. [c] The d¹⁰s⁰ configuration is an excited state of the atomic metal fragment.

symmetric complexes M(NH₃)₂ and M(PH₃)₂ or D_{∞h}-symmetric complexes M(CO)₂. However, numerous significantly smaller angles appear throughout Table 1 as well, where the symmetry of the complexes is lowered to C_{2v}. For instance, the complexes become increasingly bent when the ligands are varied along NH₃ (a strong σ donor), PH₃ (a σ donor and π acceptor) and CO (a strong π acceptor). This is most clearly seen for the group 9 complexes, where, for example, the angle decreases along Rh(NH₃)₂⁻, Rh(PH₃)₂⁻ and Rh(CO)₂⁻ from 180.0° to 141.2° and 130.8° (Figure 2). In a later section, we will show that the π-backbonding properties of the complexes constitute a prominent part of the explanation of why d¹⁰-ML₂ complexes can adopt nonlinear geometries. The increasingly strong π backbonding along this series also results in stronger metal–ligand bonds (see Table 2 for bond dissociation energies (BDEs) and Table 3 for energy decomposition analyses (EDA) results for ML complexes).

The extent of bending systematically decreases when the π-backbonding capability of the metal center decreases from the group 9 anions, via neutral group 10 atoms, to the group 11 cations. This is clearly displayed by the series of isoelectronic complexes Rh(CO)₂⁻, Pd(CO)₂ and Ag(CO)₂⁺ along which the L–M–L angle increases from 130.8° to 155.6° to 180° (Table 1).

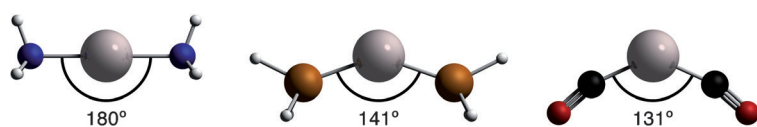


Figure 2. Equilibrium geometries computed at ZORA-BLYP/TZ2P. From left to right: Rh(NH₃)₂⁻, Rh(PH₃)₂⁻ and Rh(CO)₂⁻.

The data in Table 3 for the corresponding monocoordinate RhCO⁻, PdCO and AgCO⁺ nicely show how along this series the distortive π-orbital interactions ΔE_{oi}^π indeed become weaker, from -120 to -51 to -11 kcal mol⁻¹, respectively. In the case of group 9 metals, both phosphine and carbonyl complexes are bent, whereas, for group 10 metals, only the carbonyl complexes deviate from linearity. Complexes with a metal center from group 11 all have a linear L–M–L configuration. The reduced π backbonding also leads to weaker metal–ligand bonds. For the cationic metal centers, for which π backdonation plays a much smaller role, the metal–ligand BDEs decrease in the order NH₃ > PH₃ > CO (see Table 2). This trend originates directly from the σ-donating capabilities of the ligands as reflected

by the energy of the lone-pair orbital ε(LP), which decreases in this order (see Table 4). Note that, for the same reason, the basicity of the ligand as measured by the proton affinity (PA) decreases along NH₃ > PH₃ > CO.^[26] For the anionic group 9 metal centers, the opposite order is found, that is, metal–ligand BDEs decrease in the order CO > PH₃ > NH₃, following the π-accepting capabilities of the ligands.

Linearity also increases if one descends in a group. For example, from Ni(CO)₂ to Pd(CO)₂ to Pt(CO)₂, the L–M–L angle increases from 144.5° to 155.6° to 159.0°. Interestingly, this last trend is opposite to what one would expect proceeding from a steric model. If one goes from a larger to a smaller metal center, that is, going up in a group, the ligands are closer to each other and thus experience stronger mutual steric repulsion. But instead of becoming more linear to avoid such repulsion, the complexes bend even further in the case of the smaller metal. For example, when the palladium atom in Pd(CO)₂ is replaced by a smaller nickel atom, the L–M–L angle decreases from 155.6° in Pd(CO)₂ to 144.5° in Ni(CO)₂. Later on, we show that this seemingly counterintuitive trend also originates from enhanced π backbonding which dominates the increased steric repulsion.

General bonding mechanism

The bending of our model complexes can be understood in terms of a monocoordinate complex to which a second ligand is added either in a linear or a bent arrangement, ML + L → ML₂ (see below). Using Pd(CO)₂ as an example, we start from a PdCO fragment, and consider the addition of the second CO

Table 3. Energy decomposition analyses [kcal mol⁻¹] and orbital energies ϵ [eV] for the metal–ligand bonds in monoligated transition-metal complexes M–L.^[a]

| ML | ΔE | ΔE_{int} | ΔV_{elstat} | ΔE_{Pauli} | ΔE_{oi} | $\Delta E_{\text{oi}}^{\sigma}$ | $\Delta E_{\text{oi}}^{\pi(b)}$ | $\epsilon[d_{\sigma}]$ | $\epsilon[d_{\pi}]$ | $\epsilon[d_{\delta}]$ |
|--------------------------------|------------|-------------------------|----------------------------|---------------------------|------------------------|---------------------------------|---------------------------------|------------------------|---------------------|------------------------|
| CoNH ₃ ⁻ | -217.1 | -218.4 | -110.0 | 166.3 | -274.7 | -241.8 | -32.9 | +1.84 | +2.91 | +3.99 |
| CoPH ₃ ⁻ | -240.6 | -241.7 | -197.9 | 204.5 | -248.2 | -123.9 | -124.4 | +1.67 | +1.81 | +3.38 |
| CoCO ⁻ | -280.6 | -286.4 | -233.4 | 274.5 | -327.5 | -141.7 | -185.8 | +1.34 | +1.17 | +3.20 |
| RhNH ₃ ⁻ | -55.5 | -56.2 | -143.2 | 202.1 | -115.1 | -110.8 | -4.3 | +1.72 | +1.83 | +2.53 |
| RhPH ₃ ⁻ | -89.9 | -90.3 | -269.7 | 311.7 | -132.3 | -61.7 | -70.6 | +1.49 | +0.91 | +2.20 |
| RhCO ⁻ | -122.0 | -126.0 | -273.3 | 364.1 | -216.8 | -96.7 | -120.1 | +1.05 | -0.09 | +1.56 |
| IrNH ₃ ⁻ | -85.0 | -85.8 | -196.9 | 268.9 | -157.8 | -142.9 | -14.9 | +1.54 | +2.16 | +2.91 |
| IrPH ₃ ⁻ | -126.5 | -127.2 | -349.2 | 396.0 | -174.1 | -85.9 | -88.2 | +1.18 | +0.73 | +2.28 |
| IrCO ⁻ | -166.3 | -171.3 | -353.5 | 461.5 | -279.2 | -129.6 | -149.7 | +0.63 | -0.26 | +1.68 |
| NiNH ₃ | -77.0 | -77.3 | -116.2 | 139.8 | -100.8 | -94.5 | -6.3 | -3.28 | -2.99 | -2.21 |
| NiPH ₃ | -88.0 | -88.7 | -161.3 | 173.3 | -100.7 | -50.8 | -49.9 | -3.79 | -3.93 | -2.90 |
| NiCO | -109.3 | -110.4 | -171.6 | 210.3 | -149.1 | -60.4 | -88.7 | -4.89 | -5.40 | -4.14 |
| PdNH ₃ | -21.6 | -21.7 | -88.0 | 105.1 | -38.8 | -34.5 | -4.4 | -3.46 | -3.81 | -3.47 |
| PdPH ₃ | -39.4 | -39.8 | -166.2 | 190.3 | -63.8 | -35.3 | -28.5 | -4.49 | -5.29 | -4.56 |
| PdCO | -47.4 | -47.8 | -161.4 | 213.3 | -99.7 | -48.0 | -51.8 | -5.28 | -6.48 | -5.53 |
| PtNH ₃ | -50.1 | -50.4 | -170.1 | 211.4 | -91.7 | -82.0 | -9.7 | -4.19 | -4.46 | -3.72 |
| PtPH ₃ | -77.3 | -78.9 | -273.9 | 310.3 | -115.3 | -70.5 | -44.8 | -4.92 | -5.72 | -4.53 |
| PtCO | -87.9 | -88.7 | -271.6 | 356.9 | -174.0 | -91.6 | -82.4 | -5.97 | -7.28 | -5.77 |
| CuNH ₃ ⁺ | -70.0 | -70.1 | -104.5 | 86.0 | -51.7 | -41.9 | -9.8 | -11.80 | -12.13 | -12.02 |
| CuPH ₃ ⁺ | -68.7 | -73.5 | -101.7 | 94.0 | -65.8 | -51.8 | -14.0 | -11.99 | -12.44 | -12.15 |
| CuCO ⁺ | -50.2 | -50.3 | -89.8 | 100.7 | -61.2 | -38.8 | -22.4 | -13.7 | -14.28 | -13.90 |
| AgNH ₃ ⁺ | -48.7 | -48.7 | -73.3 | 58.8 | -34.2 | -28.5 | -5.8 | -12.56 | -13.60 | -13.57 |
| AgPH ₃ ⁺ | -47.9 | -51.8 | -84.3 | 81.3 | -48.8 | -39.9 | -8.9 | -12.41 | -13.67 | -13.85 |
| AgCO ⁺ | -28.4 | -28.6 | -59.1 | 67.2 | -36.7 | -26.2 | -10.6 | -14.08 | -15.07 | -14.86 |
| AuNH ₃ ⁺ | -71.4 | -71.6 | -124.8 | 123.2 | -70.0 | -60.3 | -9.7 | -12.49 | -13.32 | -12.92 |
| AuPH ₃ ⁺ | -84.2 | -91.0 | -177.9 | 187.2 | -100.3 | -80.9 | -19.4 | -12.52 | -13.70 | -13.06 |
| AuCO ⁺ | -55.0 | -55.1 | -149.0 | 188.4 | -94.5 | -64.9 | -29.7 | -14.20 | -15.53 | -14.73 |

[a] Computed at ZORA-BLYP/TZ2P. See [Eqs. (1)–(3)]. [b] Also includes small contributions from δ orbital interactions, which can only be separated for C_{∞v}-symmetric MCO complexes. There, the δ term amounts at most to 3.5% of the π term.

Table 4. Ligand orbital energies ϵ [eV] and proton affinities [kcal mol⁻¹].^[a]

| | $\epsilon(\text{LP})$ | $\epsilon(\pi^*)$ | PA |
|-----------------|-----------------------|-------------------|--------|
| NH ₃ | -6.05 | +1.42 | +201.4 |
| PH ₃ | -6.63 | -0.24 | +185.2 |
| CO | -8.93 | -1.92 | +141.5 |

[a] Computed at ZORA-BLYP/TZ2P. LP: lone pair, π^* : acceptor orbital. Proton affinities (PA) from enthalpies at 298.15 K and 1 atm.

ligand both at a 180° angle and a 90° angle. Our Kohn–Sham MO analyses show that, in PdCO, the degeneracy of the five occupied d orbitals on palladium is lowered by interactions with the ligand (see Figure 3). Choosing the M–L bond along the z axis, the d_{xz} and d_{yz} orbitals act as donor orbitals for π backdonation into the two π^* -acceptor orbitals on the CO ligand, resulting in two stabilized “d _{π} ” orbitals at -6.5 eV (value not shown in Figure 3). The d_{xy} and d_{x²-y²} (or “d _{δ} ”) orbitals at -5.5 eV do not overlap and interact with the ligand. The d_{z²} orbital is destabilized due to the antibonding overlap

with the lone pair on the ligand, resulting in a “d _{σ} ” orbital that is relatively high in energy, at -5.3 eV.

When the second CO ligand coordinates opposite the first one (i.e., in a linear L–M–L arrangement), its π^* -acceptor orbitals interact with the d _{π} orbitals on the PdCO fragment. The latter are already considerably stabilized by π backdonation to the first CO ligand (Figure 3B, left). When, instead, the second ligand is added at an angle of 90°, its π^* orbitals overlap with only one d _{π} orbital, and with one d _{δ} orbital (Figure 3B, right). This d _{δ} orbital is essentially a pure metal d orbital that has *not* yet been stabilized by any coordination bond. Consequently, this orbital has a higher energy and is, therefore, a more capable donor orbital for π backdonation into the π^* orbital of the second CO ligand. This results in a stronger, more stabilizing donor–acceptor interaction of this pair of orbitals in the 90° (Figure 3A, right) than in the 180° ML₂ geometry (Figure 3A, left: cf. red-highlighted π interactions). σ -Donation interactions are affected less by bending. It is therefore π backdonation that favors bending. The more detailed energy decomposition analyses in the following sections consolidate this picture.

Bonding mechanism: Variation of ligands

To understand the trends in nonlinearity of our ML₂ complexes (see above and Table 1), we have quantitatively analyzed the metal–ligand bonding between ML and the second ligand L as a function of the L–M–L angle. The results are collected in Table 2 and displayed in Figure 4–7. Most of our model complexes have a d¹⁰-type ground-state configuration but not all of them, as indicated in detail in Table 2. Yet, *all* model systems discussed here have been kept in d¹⁰-configuration, to achieve a consistent comparison and because, on the longer term, we are interested in understanding more realistic dicoordinated d¹⁰-transition-metal complexes that feature, for example, as catalytically active species in metal-mediated bond activation. We start in all cases from the optimal *linear* ML₂ structure (i.e., the complex optimized in either D_{∞h} or D_{3h} symmetry) and then analyze the bonding between ML and L' as a function of

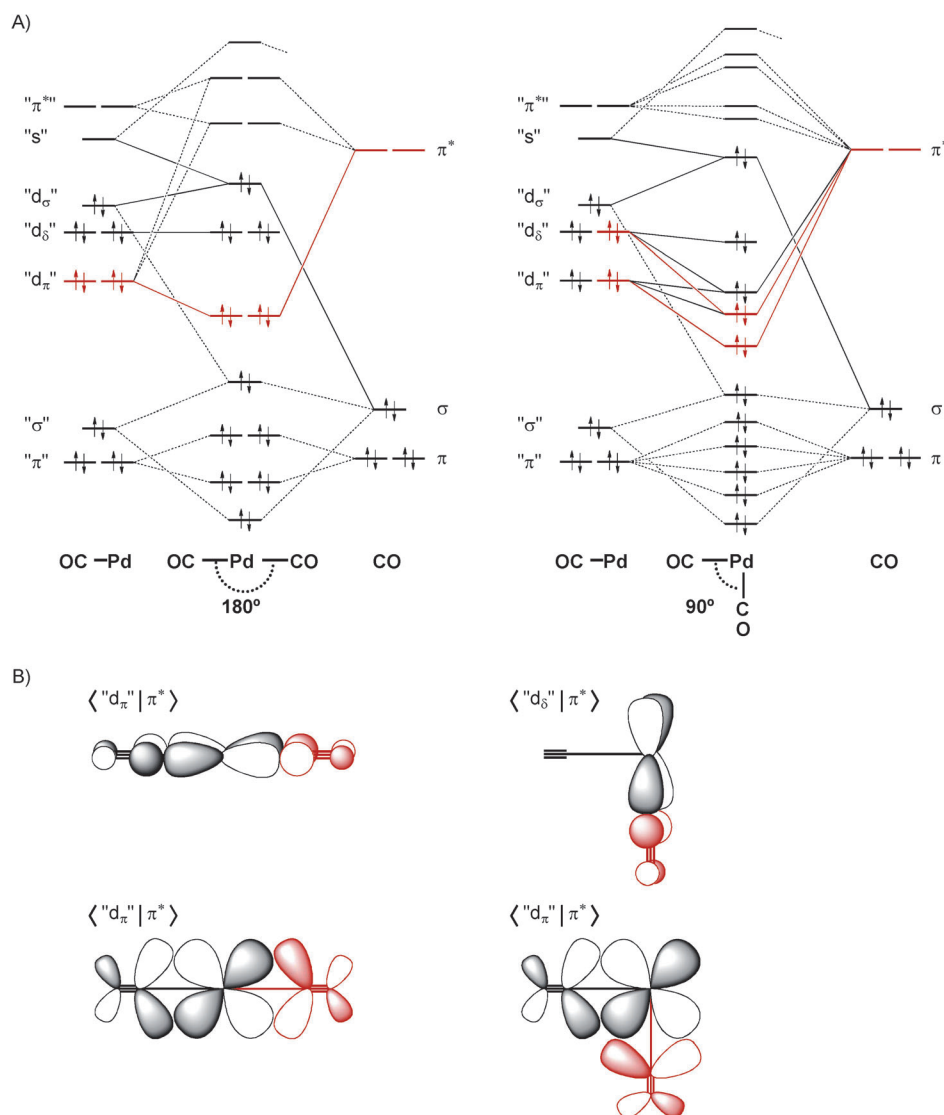


Figure 3. A) Schematic MO diagrams for the bonding mechanism between PdCO and CO in linear Pd(CO)₂ (left) and at a L–M–L angle of 90° (right): dominant interactions (—), other interactions (---), π backbonding (—). B) Schematic representation of the bonding overlaps of the donating orbital on PdCO (black) with the π -accepting orbital on the second CO ligand (red).

the L–M–L angle, from 180° to 90°, while keeping all other geometry parameters frozen. The analyses were done in C_s symmetry, bending the complexes in the mirror plane, with the out-of-plane hydrogen atoms of M(NH₃)₂ and M(PH₃)₂ towards each other. Thus, we are able to separate the orbital interactions symmetric to the mirror plane (A' irrep) from the orbital interactions asymmetric to the mirror plane (A'' irrep): $\Delta E_{oi}(\zeta) = \Delta E_{oi}^{A'}(\zeta) + \Delta E_{oi}^{A''}(\zeta)$ [Eq. (3)]. The use of frozen fragment geometries allows us to study purely how the interaction energy changes as the angle is varied, without any perturbation due to geometrical relaxation. Therefore, any change in ΔE stems exclusively from a change in $\Delta E_{int} = \Delta V_{elstat} + \Delta E_{Pauli} + \Delta E_{oi}^{A'} + \Delta E_{oi}^{A''}$. Note that rigid bending of the linearly optimized L–M–L complexes causes minima on the energy profiles to shift to larger angles than in fully optimized complexes, but this does not alter any relative structural or energy order.

In Figure 4, we show the energy decomposition analyses [Eq. (2)] and how they vary along the palladium complexes Pd(NH₃)₂, Pd(PH₃)₂ and Pd(CO)₂. Upon bending the LM–L' complex from 180° to 90°, the average distance between the electron density on LM and the nuclei of L' decreases (the Pd–P distance however remains constant), which results in a more stabilizing electrostatic attraction ΔV_{elstat} . Likewise, the Pauli repulsion ΔE_{Pauli} increases because of a larger overlap of the lone pair on L' with the d_{z²}-derived d_σ orbital on the ML fragment. The latter is the antibonding combination of the metal d_{z²} orbital and the ligand lone pair, with a fair amount of metal s character admixed in an L–M bonding fashion. The resulting hybrid orbital is essentially the d_{z²} orbital with a relatively large torus. The increase in Pauli repulsion that occurs as the L–M–L' angle decreases stems largely from the overlap of the lone pair on the second ligand L' with this torus. For Pd(CO)₂ for example, the overlap of the L' lone pair with the d_σ hybrid orbital on ML increases from 0.05 to 0.28 upon bending from 180° to 90°. We note that this repulsion induces a secondary relaxation, showing up as a stabilizing $\Delta E_{oi}^{A'}$, by which it is largely canceled again. The mechanism through

which this relief of Pauli repulsion happens is that, in the antibonding combination with the L' lone pair, the d_σ orbital is effectively pushed up in energy and (through its L'-lone-pair component) interacts in a stabilizing fashion with the metal s-derived LUMO on ML.

The aforementioned π backbonding that favors bending (see Figure 3) shows up in an increased stabilization in the asymmetric $\Delta E_{oi}^{A''}$ component as the L–M–L angle decreases. To more clearly reveal the role of the orbital interactions within A'' symmetry, we separate the interaction energy ΔE_{int} into the corresponding term $\Delta E_{oi}^{A''}$ plus the remaining interaction energy ΔE_{intr} which combines the other interaction terms comprising electrostatic attraction ΔV_{elstat} , Pauli repulsion ΔE_{Pauli} and the symmetric orbital interactions $\Delta E_{oi}^{A'}$:

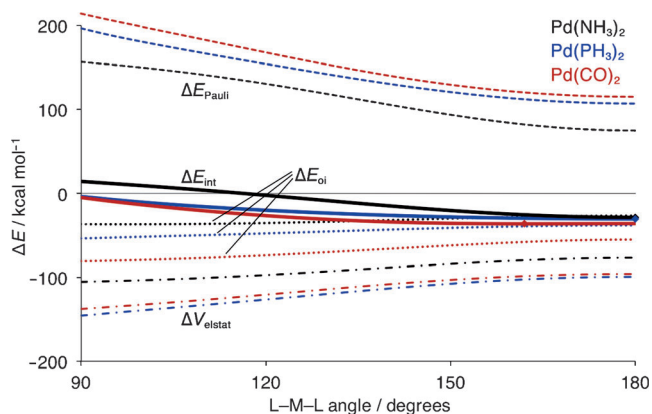


Figure 4. Energy decomposition analysis [Eq. (2)] of the interaction between PdL and L in dicoordinated palladium complexes PdL₂ as a function of the L–M–L angle (L = NH₃, PH₃, CO).

$$\begin{aligned} \Delta E_{\text{int}}(\zeta) &= \Delta V_{\text{elstat}}(\zeta) + \Delta E_{\text{Pauli}}(\zeta) + \Delta E_{\text{oi}}^{A'}(\zeta) + \Delta E_{\text{oi}}^{A''}(\zeta) \\ &= \Delta E'_{\text{int}}(\zeta) + \Delta E_{\text{oi}}^{A''}(\zeta) \end{aligned} \quad (4)$$

Thus, the interaction energy is split into two contributions which are both stabilizing along a large part of the energy profiles studied and which vary over a significantly smaller range. Therefore, this decomposition allows us to directly compare the importance of $\Delta E_{\text{oi}}^{A''}$ with respect to the combined influence of all other terms, contained in $\Delta E'_{\text{int}}$. The latter contains the aforementioned counteracting and largely canceling terms of strong Pauli repulsion between A' orbitals and the resulting stabilizing relaxation effect $\Delta E_{\text{oi}}^{A'}$.

The results of this alternative decomposition appear in Figure 5, again for the series of palladium complexes Pd(NH₃)₂, Pd(PH₃)₂ and Pd(CO)₂. In each of these complexes, bending begins at a certain point to weaken the $\Delta E'_{\text{int}}$ energy term and, at smaller L–M–L angles, makes it eventually repulsive as the Pauli repulsion term becomes dominant (see also Figure 4). Numerical experiments, in which we consider the rigid bending process of a complex in which the metal is removed, show that steric repulsion between ligands does contribute to this

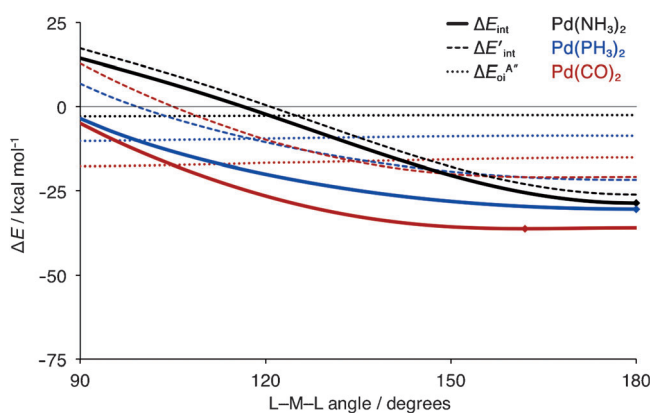


Figure 5. Energy decomposition analysis [Eq. (4)] of the interaction between PdL and L in dicoordinated palladium complexes PdL₂ as a function of the L–M–L angle (L = NH₃, PH₃, CO).

repulsion, especially at smaller angles. Thus, direct Pauli repulsion between L and L' in LM–L' goes, upon bending from 180° to 90°, from 0.3 to 4.6 kcal mol⁻¹ for Pd(NH₃)₂ and from 0.4 to 9.0 kcal mol⁻¹ for Pd(CO)₂ (data not shown in Figures). This finding confirms that ligands avoid each other for steric reasons, but it also shows that the effect is small as compared to the overall change in the ΔE_{int} curves (see Figure 5). The dominant term that causes ΔE_{int} to go up in energy upon bending is the increasing Pauli repulsion that occurs as the L' lone pair overlaps more effectively with the LM d_σ orbital.

In a number of cases, the stabilization upon bending from the asymmetric orbital interactions $\Delta E_{\text{oi}}^{A''}$ dominates the destabilization from the $\Delta E'_{\text{int}}$ term. These cases are the complexes that adopt nonlinear equilibrium geometries. This $\Delta E_{\text{oi}}^{A''}$ term gains stabilization upon bending LM–L' because the π*-acceptor orbital on the ligand L' moves from a position in which it can overlap with a ligand-stabilized LM d_π orbital to a more or less pure metal and, thus, up to 1 eV higher-energy d_σ orbital (see Table 3), which leads to a more stabilizing donor–acceptor orbital interaction (see Figure 5). The gain in stabilization of $\Delta E_{\text{oi}}^{A''}$ upon bending and, thus, the tendency to bend increases along NH₃ to PH₃ to CO. The reason is the increasing π-accepting ability of the ligands as reflected by the energy $\epsilon(\pi^*)$ of the ligands' π* orbital which is lowered from +1.42 to -0.24 to -1.92 eV, respectively (see Table 4). Thus, for Pd(NH₃)₂, where π backdonation plays essentially no role, the $\Delta E_{\text{oi}}^{A''}$ term is stabilized by less than 0.5 kcal mol⁻¹ if we go from 180° to 90°. For PH₃, known as a moderate π-accepting ligand, this energy term is stabilized by 1.5 kcal mol⁻¹ from 180° to 90° and, for CO, this stabilization amounts to 2.5 kcal mol⁻¹. Thus, in the case of palladium complexes, the energy profile for bending the complexes becomes progressively more flat as the ligands are better π acceptors, but only the carbonyl ligand generates sufficient stabilization through increased π-backbonding in $\Delta E_{\text{oi}}^{A''}$ to shift the equilibrium geometry to an angle smaller than 180°.

Bonding mechanism: Variation of metals

Applying the same analysis along the series Rh(CO)₂⁻, Pd(CO)₂ and Ag(CO)₂⁺, reveals a similar but clearer picture (Figure 6). Along this series of isoelectronic complexes, the equilibrium geometries have L–M–L angles of 130.8°, 155.6° and 180.0°. Similar to the results obtained for the series discussed above, we again find a $\Delta E'_{\text{int}}$ term that is relatively shallow and eventually, at small angles, dominated by the Pauli repulsion. The $\Delta E'_{\text{int}}$ term does not provide additional stabilization upon bending the complex. We do observe, however, a $\Delta E_{\text{oi}}^{A''}$ component that, from Rh(CO)₂⁻ to Pd(CO)₂ to Ag(CO)₂⁺, becomes more stabilizing and also gains more stabilization upon bending from 180° to 90°. That is, whereas for Ag(CO)₂⁺ the $\Delta E_{\text{oi}}^{A''}$ remains constant at a value of -5.4 kcal mol⁻¹ as the complex is bent from 180° to 90°; the same component for Pd(CO)₂ starts already at a more stabilizing value of -15.1 kcal mol⁻¹ at 180° and is stabilized more than 2.5 kcal mol⁻¹ as the complex is bent to 90°. For Rh(CO)₂⁻, the effect of the additional stabilization upon bending is strongest, almost 10 kcal mol⁻¹, as $\Delta E_{\text{oi}}^{A''}$

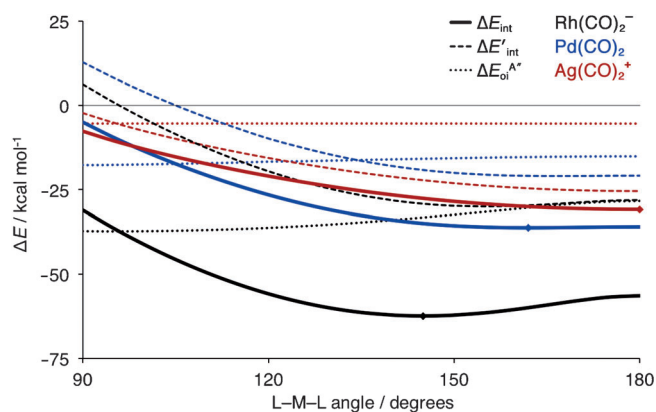


Figure 6. Energy decomposition analysis [Eq. (4)] of the interaction between MCO and CO in dicarbonyl-transition-metal complexes $M(\text{CO})_2$ as a function of the L–M–L angle ($M = \text{Rh}^-$, Pd, Ag^+).

goes from $-28.4 \text{ kcal mol}^{-1}$ at 180° to $-37.3 \text{ kcal mol}^{-1}$ at 90° . The mechanism behind this trend is that the donor capability of the metal d orbitals increases as they are pushed up in energy from the cationic AgCO^+ to the neutral PdCO to the negative RhCO^- (see Table 3). This trend of increasing d orbital energies leads to a concomitant strengthening π backdonation and, thus, an increasing energy difference in the LM fragment between the pure metal d_δ and the ligand-stabilized d_π orbitals. Thus, the “fresh” d_δ orbitals are higher in energy than the ligand-stabilized d_π orbitals by 0.21 to 0.96 to 1.65 eV along AgCO^+ , PdCO and RhCO^- , respectively (see Table 3). Consequently, the LM–L’ complexes benefit progressively along this series from increasing the overlap of L’ π^* with the higher-energy d_δ orbitals in the bent geometry.

Variation of the metal down a group goes with a less pronounced increase of the L–M–L angle that originates from more subtle changes in the bonding mechanism. The largest variation in bite angle is observed along the group 10 complexes $\text{Ni}(\text{CO})_2$, $\text{Pd}(\text{CO})_2$ and $\text{Pt}(\text{CO})_2$ which show L–M–L angles of 144.5° , 155.6° and 159.0° , respectively (see Table 1). Two factors lie behind this trend: (1) a weakening in π backbonding as the metal orbital energy decreases from nickel 3d to palladium 4d; (2) a steeper increase upon bending in Pauli repulsion between PtCO d_σ (that has a large torus due to strong admixture of the relativistically stabilized Pt 6s AO) and the lone pair of the other CO ligand. As shown in Figure 7, the π -backbonding stabilization of $\Delta E_{\text{oi}}^{\text{A}^*}$ upon bending is indeed stronger for $\text{Ni}(\text{CO})_2$ than for $\text{Pd}(\text{CO})_2$ and $\text{Pt}(\text{CO})_2$. The difference between the latter is small because the greater (more favorable) overlap of the π^* orbitals on the ligand with the more extended platinum d orbitals on PtCO compensates for the lower (less favorable) platinum d orbital energy. Figure 7 also shows how the $\Delta E'_{\text{int}}$ term containing the aforementioned Pauli repulsion becomes more rapidly destabilizing at smaller angles for $\text{Pt}(\text{CO})_2$ than for $\text{Ni}(\text{CO})_2$ and $\text{Pd}(\text{CO})_2$. Likewise, in the case of group 9 complexes, the more steeply increasing Pauli repulsion of the ligand lone pair with the large iridium d_σ torus pushes the equilibrium L–M–L angle of $\text{Ir}(\text{CO})_2^-$ (134.2°) to a larger value than for $\text{Rh}(\text{CO})_2^-$ (130.8° ; see Table 1). Interestingly, here, the

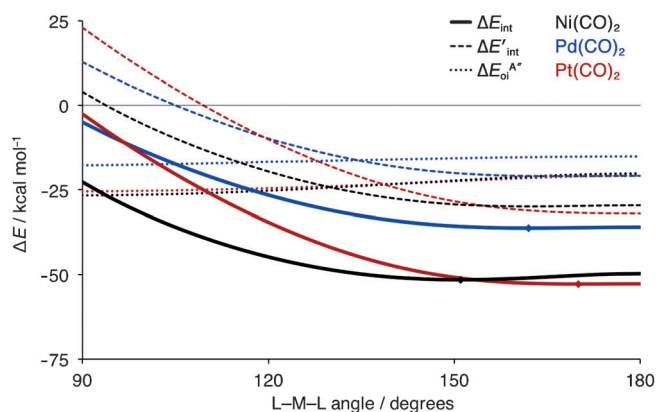


Figure 7. Energy decomposition analysis [Eq. (4)] of the interaction between MCO and CO in dicarbonyl-transition-metal complexes $M(\text{CO})_2$ as a function of the L–M–L angle ($M = \text{Ni}$, Pd, Pt).

linearization energy ΔE_{lin} is nevertheless higher for the less bent $\text{Ir}(\text{CO})_2^-$ ($13.4 \text{ kcal mol}^{-1}$) than for $\text{Rh}(\text{CO})_2^-$ ($10.2 \text{ kcal mol}^{-1}$) because of the more favorable π -backbonding overlap between IrCO^- and CO (see Table 1). This illustrates the subtlety of the interplay between the two features in the bonding mechanism.

Walsh diagrams

Based on detailed Kohn–Sham MO analyses of individual complexes, we have constructed generalized Walsh diagrams corresponding to bending the ML_2 complexes from 180° to 90° . This choice comes down to an alternative perspective on the same problem, and the emerging electronic mechanism, why bending may occur, is fully equivalent to the one obtained in the above analyses based on two interacting fragments LM + L’, namely: Bending ML_2 to a nonlinear geometry enables ligand π^* orbitals (if they are available on L) to overlap with and stabilize metal d orbitals that are not stabilized in the linear arrangement. The spectrum of different bonding situations has been summarized in two simplified diagrams that correspond to two extreme situations: weakly π -accepting ligands (Figure 8A) and strongly π -accepting ligands (Figure 8B). In these diagrams, we position the d_{z^2} orbital in linear ML_2 above the other d orbitals, a situation that occurs, for example, for $\text{Pd}(\text{PH}_3)_2$. The relative position of the d_{z^2} may change, and in some complexes, such as, $\text{Rh}(\text{NH}_3)_2^-$, it is located below the other d orbitals. These variations do not affect the essential property of the orbitals, namely, their change in energy upon bending the ML_2 complex. Furthermore, we speak about weakly π -accepting ligands, not just about (purely) σ -donating ligands, because it turns out that none of our model ligands has negligible π -accepting capability. The resulting Walsh diagrams summarize our results in a more easy to use pictorial manner which, in particular for the situation with strongly π -accepting ligands, is novel.

We first examine the diagram with weakly π -accepting ligands (Figure 8A). Bending ML_2 from linear to nonlinear significantly destabilizes the d_{z^2} orbital because of turning on over-

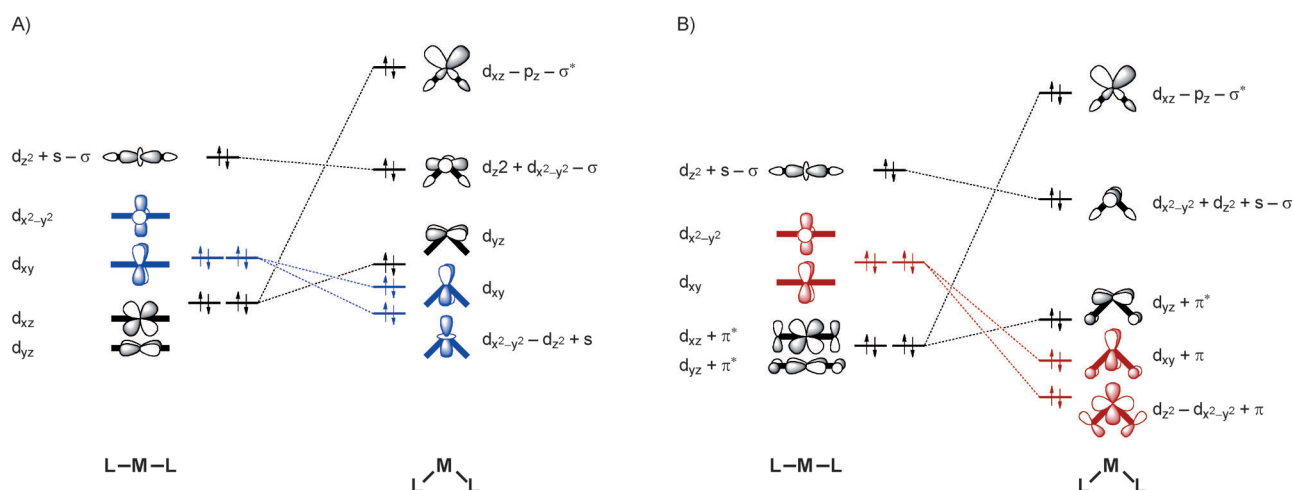


Figure 8. Simplified Walsh diagrams for bending ML_2 complexes that emerge from our Kohn–Sham MO analyses (+/– indicate bonding/antibonding) A) without and B) with π backbonding.

lap with the out-of-phase combination of ligand lone pairs. This effect is related to the overlap between the LM d_σ torus and the L' lone pair in the fragment approach (see above). At small angles, direct ligand–ligand antibonding becomes important. The d_{z^2} orbital is slightly stabilized in the nonlinear situation due to a decreasing antibonding overlap with the in-phase combination of ligand lone pairs, augmented by admixing with the $d_{x^2-y^2}$ orbital (see a detailed scheme of this intermixing in Figure S1 of the Supporting Information). Note that if our model ligands would have been purely σ donating, the d_{xz} , d_{yz} and d_{xy} levels would not be affected by $L-M-L$ bending. Yet, they are, although only slightly so. This is a manifestation of some π backbonding, which is discussed in more detail below for the strongly π -accepting ligands.

In the case of strongly π -accepting orbitals (Figure 8B), bending ML_2 from linear to nonlinear still goes with significant destabilization of d_{xz} and slight stabilization of d_{z^2} (for the same reasons as discussed above for weakly π -accepting ligands). π Backbonding stabilizes both d_{xz} and d_{yz} in the linear $L-M-L$ arrangement; bending reduces π overlap which causes also d_{yz} to increase in energy. A striking phenomenon in the ML_2 Walsh diagram with strongly π -accepting ligands is the significant stabilization of the $d_{x^2-y^2}$ and d_{xy} orbitals that occurs as bending moves ligand π^* orbitals in the right orientation for π -accepting overlap with these orbitals. The resulting stabilization, if strong enough, can overcome the destabilization of the d_{xz} orbital and accounts for the observed bent complexes described in this work. This effect is related to the overlap between the LM d_δ orbital and the L' π^* in the fragment approach (see above). The same effect also nicely accounts for the nonlinear structures observed in earlier studies for d^0 metal complexes with π -donating ligands.^[27,28,29,30,31] For these complexes, a π -bonding mechanism has been proposed in which bending is favorable because it effectively increases the number of d orbitals that have non-zero overlap with the π -donating orbitals on the ligands.^[28]

Conclusion

Dicoordinated d^{10} -transition-metal complexes ML_2 can very well adopt nonlinear geometries with bite angles that deviate significantly from the usually expected 180° . This follows from our relativistic density functional theory (DFT) computations on a broad range of archetypal d^{10} - ML_2 model systems. The smallest bite angle encountered in our exploration among 27 model systems amounts to 128.6° for $Co(CO)_2^-$.

Nonlinear geometries appear to be a direct consequence of π backbonding. The geometry of d^{10} - ML_2 complexes results from two opposing features in the bonding mechanism, which we have analyzed in terms of the interaction between ML and L as a function of the $L-M-L$ angle using quantitative molecular orbital (MO) theory and energy decomposition analyses: Bending destabilizes the interaction ΔE_{int} between ML and L through increasing steric (Pauli) repulsion between the ligands' lone-pair orbital lobes as well as a destabilization, by the latter, of the ML d_σ hybrid orbital; however, bending *can also stabilize* ΔE_{int} because of enhanced π backdonation. The reason is that the π -acceptor orbital on the ligand L (e.g., $CO \pi^*$) interacts in the linear arrangement with an already stabilized ML d_π hybrid orbital, whereas in the bent geometry, it enters into a more favorable donor–acceptor orbital interaction with an unstabilized, that is, higher-energy metal d_δ orbital.

Our analyses complement the existing text-book Walsh diagram for bending ML_2 complexes^[8] with a variant that includes metal–ligand π backbonding. Our findings also contribute to a more rational design of catalytically active and selective ML_2 complexes.^[1,32]

Acknowledgements

We thank the National Research School Combination-Catalysis (NRSC-C) and the Netherlands Organization for Scientific Research (NWO-CW and NWO-EW) for financial support.

Keywords: bond theory · density functional calculations · energy decomposition analysis · molecular geometry · transition-metal complexes · π backdonation

- [1] See, for example: a) J. F. Hartwig, *Organotransition Metal Chemistry: From Bonding to Catalysis*, 1st ed., University Science Books, Sausalito, **2010**; b) P. W. N. M. van Leeuwen, P. C. J. Kamer, J. N. H. Reek, P. Dierkes, *Chem. Rev.* **2000**, *100*, 2741; c) M.-N. Birkholz née Gensow, Z. Freixa, P. W. N. M. van Leeuwen, *Chem. Soc. Rev.* **2009**, *38*, 1099; d) W.-J. van Zeist, F. M. Bickelhaupt, *Dalton Trans.* **2011**, *40*, 3028.
- [2] S. Otsuka, *J. Organomet. Chem.* **1980**, *200*, 191.
- [3] M. A. Carvajal, J. J. Novoa, S. Alvarez, *J. Am. Chem. Soc.* **2004**, *126*, 1465.
- [4] R. B. King, *Coord. Chem. Rev.* **2000**, *197*, 141.
- [5] T. Ziegler, *Inorg. Chem.* **1985**, *24*, 1547.
- [6] S. Otsuka, T. Yoshida, M. Matsumoto, K. Nakatsu, *J. Am. Chem. Soc.* **1976**, *98*, 5850.
- [7] E. Dinjus, W. Leitner, *Appl. Organomet. Chem.* **1995**, *9*, 43.
- [8] T. A. Albright, J. K. Burdett, M. H. Whangbo, *Orbital Interactions in Chemistry*, John Wiley & Sons, New York, **1985**.
- [9] a) R. J. Gillespie, R. S. Nyholm, *Q. Rev. Chem. Soc.* **1957**, *11*, 339; b) R. J. Gillespie, *J. Chem. Educ.* **1963**, *40*, 295.
- [10] a) R. J. Gillespie, *Chem. Soc. Rev.* **1992**, *21*, 59; b) R. J. Gillespie, *Coord. Chem. Rev.* **2008**, *252*, 1315.
- [11] G. te Velde, F. M. Bickelhaupt, E. J. Baerends, C. Fonseca Guerra, S. J. A. van Gisbergen, J. G. Snijders, T. Ziegler, *J. Comput. Chem.* **2001**, *22*, 931.
- [12] C. Fonseca Guerra, J. G. Snijders, G. te Velde, E. J. Baerends, *Theor. Chem. Acc.* **1998**, *99*, 391–403.
- [13] E. J. Baerends, T. Ziegler, J. Autschbach, D. Bashford, A. Bérces, F. M. Bickelhaupt, C. Bo, P. M. Boerrigter, L. Cavallo, D. P. Chong, L. Deng, R. M. Dickson, D. E. Ellis, M. van Faassen, L. Fan, T. H. Fischer, C. Fonseca Guerra, A. Ghysels, A. Giammona, S. J. A. van Gisbergen, A. W. Götz, J. A. Groeneveld, O. V. Gritsenko, M. Grüning, S. Gusarov, F. E. Harris, P. van den Hoek, C. R. Jacob, H. Jacobsen, L. Jensen, J. W. Kaminski, G. van Kessel, F. Kootstra, A. Kovalenko, M. V. Krykunov, E. van Lenthe, D. A. McCormack, A. Michalak, M. Mitoraj, J. Neugebauer, V. P. Nicu, L. Noodleman, V. P. Osinga, S. Patchkovskii, P. H. T. Philipsen, D. Post, C. C. Pye, W. Ravenek, J. I. Rodríguez, P. Ros, P. R. T. Schipper, G. Schreckenbach, J. S. Seldenthuis, M. Seth, J. G. Snijders, M. Solà, M. Swart, D. Swerhone, G. te Velde, P. Vernooijs, L. Versluis, L. Visscher, O. Visser, F. Wang, T. A. Wesolowski, E. M. van Wezenbeek, G. Wiesenecker, S. K. Wolff, T. K. Woo, A. L. Yakovlev, *ADF2010, SCM, Theoretical Chemistry*; Vrije Universiteit, Amsterdam, The Netherlands; <http://www.scm.com/>.
- [14] a) P. M. Boerrigter, G. te Velde, E. J. Baerends, *Int. J. Quantum Chem.* **1988**, *33*, 87; b) G. te Velde, E. J. Baerends, *J. Comp. Physiol.* **1992**, *99*, 84.
- [15] E. van Lenthe, E. J. Baerends, *J. Comput. Chem.* **2003**, *24*, 1142.
- [16] L. Versluis, T. Ziegler, *J. Chem. Phys.* **1988**, *88*, 322.
- [17] J. C. Slater, *Quantum Theory of Molecules and Solids*, Vol. 4, McGraw-Hill, New York, **1974**.
- [18] a) A. D. Becke, *J. Chem. Phys.* **1986**, *84*, 4524; b) A. D. Becke, *Phys. Rev. A* **1988**, *38*, 3098.
- [19] a) C. Lee, W. Yang, R. G. Parr, *Phys. Rev. B* **1988**, *37*, 785; b) B. G. Johnson, P. M. W. Gill, J. A. Pople, *J. Chem. Phys.* **1993**, *98*, 5612; c) T. V. Russo, R. L. Martin, P. J. Hay, *J. Chem. Phys.* **1994**, *101*, 7729.
- [20] a) E. van Lenthe, E. J. Baerends, J. G. Snijders, *J. Chem. Phys.* **1994**, *101*, 9783; b) E. van Lenthe, R. van Leeuwen, E. J. Baerends, J. G. Snijders, *Int. J. Quantum Chem.* **1996**, *57*, 281.
- [21] a) G. T. de Jong, M. Solà, L. Visscher, F. M. Bickelhaupt, *J. Chem. Phys.* **2004**, *121*, 9982; b) G. T. de Jong, D. P. Geerke, A. Diefenbach, F. M. Bickelhaupt, *Chem. Phys.* **2005**, *313*, 261; c) G. T. de Jong, D. P. Geerke, A. Diefenbach, M. Solà, F. M. Bickelhaupt, *J. Comput. Chem.* **2005**, *26*, 1006; d) G. T. de Jong, F. M. Bickelhaupt, *J. Phys. Chem. A* **2005**, *109*, 9685; e) G. T. de Jong, F. M. Bickelhaupt, *J. Chem. Theory Comput.* **2006**, *2*, 322.
- [22] a) A. Bérces, R. M. Dickson, L. Fan, H. Jacobsen, D. Swerhone, T. Ziegler, *Comput. Phys. Commun.* **1997**, *100*, 247; b) H. Jacobsen, A. Bérces, D. Swerhone, T. Ziegler, *Comput. Phys. Commun.* **1997**, *100*, 263; c) S. K. Wolff, *Int. J. Quantum Chem.* **2005**, *104*, 645.
- [23] W. J. van Zeist, C. Fonseca Guerra, F. M. Bickelhaupt, *J. Comput. Chem.* **2008**, *29*, 312.
- [24] F. M. Bickelhaupt, E. J. Baerends in *Reviews in Computational Chemistry*, Vol. 15 (Eds.: K. B. Lipkowitz, D. B. Boyd), Wiley-VCH, Weinheim, **2000**, pp. 1–86.
- [25] T. Ziegler, A. Rauk, *Inorg. Chem.* **1979**, *18*, 1755.
- [26] M. Swart, E. Rösler, F. M. Bickelhaupt, *J. Comput. Chem.* **2006**, *27*, 1486.
- [27] C. A. Jolly, D. S. Marynick, *Inorg. Chem.* **1989**, *28*, 2893.
- [28] M. Kaupp, *Angew. Chem.* **2001**, *113*, 3642; *Angew. Chem. Int. Ed.* **2001**, *40*, 3534.
- [29] R. J. Gillespie, I. Bytheway, R. S. DeWitte, R. F. W. Bader, *Inorg. Chem.* **1994**, *33*, 2115.
- [30] M. Kaupp, P. von R. Schleyer, *J. Am. Chem. Soc.* **1992**, *114*, 491.
- [31] M. Kaupp, *Chem. Eur. J.* **1999**, *5*, 3631.
- [32] See, for example: a) W.-J. van Zeist, R. Visser, F. M. Bickelhaupt, *Chem. Eur. J.* **2009**, *15*, 6112; b) W.-J. van Zeist, F. M. Bickelhaupt, *Org. Biomol. Chem.* **2010**, *8*, 3118.

Received: February 20, 2013

Published online on May 6, 2013